Available online at www.sciencedirect.com
SCIENCE DIRECT®
International Journal of Heat and Mass Transfer 47 (2004) 3073–3083
International Journal of HEAT and MASS TRANSFER
www.elsevier.com/locate/ijhmt

Designed porous media: maximal heat transfer density at decreasing length scales

Adrian Bejan *

Department of Mechanical Engineering and Materials Science, Duke University, Box 90300, Durham, NC 27708-0300, USA

Received 17 March 2003; received in revised form 25 February 2004

Abstract

This paper addresses the fundamental problem of maximizing the heat transfer rate density in a fixed volume in the limit of decreasing length scales. In this limit boundary layers disappear, optimized channels are no longer slender, and existing results for optimal spacings break down. Three configurations are optimized analytically based on the intersection of asymptotes method: volumes filled with parallel-plates channels, volumes filled with uniformly distributed spheres, and volumes filled with parallel plates and porous structure in each parallel-plates channel. The small-spacings asymptote is for slow Poiseuille and, respectively, Darcy flow. The large-spacings asymptote is based on heat transfer that approaches pure conduction around bodies immersed in a stationary medium. The geometric results are the optimal flow channel size, the optimal porosity of the assembly, and the maximized heat transfer rate density. The latter increases sharply as dimensions become smaller. This trend, and the method of optimizing flow architecture to achieve maximal heat transfer density, are essential in the continuing miniaturization of heat transfer devices.

Keywords: Constructal; Heat transfer density; Packing; Spacing; Porous media; Bejan number; Design; Optimization

1. Why small dimensions are needed

The key to packing maximum convective heat transfer rate per unit volume is the observation that every fluid packet and every volume element must be used for the purpose of transferring heat. Fluid flow regions that do not "work" in a heat transfer sense must be avoided. Flow regions that worked too much, and have become ineffective (filled with "used" fluid), must be eliminated. This activity of arranging and rearranging of the volumetric distribution of flow and heat transfer leads to the construction of internal structure—optimal flow architecture for maximal global performance subject to constraints. This "constructal" principle is responsible for the emergence of many flow structures in engineered and natural flow systems, as shown in two recent books [1,2].

The principle of forcing the fluid to "work" everywhere can be illustrated by considering the performance of a large volume that is filled with parallel-plates channels with forced convection. One channel is shown in Fig. 1, where the designer may contemplate two extremes. First, if the channel length L is made shorter than the thermal entrance length X_T, then the fluid that occupies the core of the duct does not participate in the heat transfer enterprise. Such fluid must not be allowed to leave the channel without having interacted thermally with the walls.

In the other extreme, when L is made longer than X_T, the fluid is so saturated with heating or cooling from the wall, that it can accommodate further heating or cooling only by overheating, i.e., by changing its bulk temperature in the downstream direction. This extreme (the fully developed regime) must be avoided. It is important to note that the decision to avoid the thermally fully developed flow regime is new relative to current trends in microscale heat exchanger design,

* Tel.: +1-919-660-5309; fax: +1-919-660-8963.
E-mail address: dalford@duke.edu (A. Bejan).

0017-9310/$ - see front matter © 2004 Elsevier Ltd. All rights reserved.
doi:10.1016/j.ijheatmasstransfer.2004.02.025

Nomenclature

A	frontal area of package (m^2)
Be_L	Bejan number, or pressure drop number based on L Eq. (2)
Be_p	porous medium Bejan number, Eq. (48)
c_p	specific heat at constant pressure ($J\,kg^{-1}\,K^{-1}$)
C_D	drag coefficient
d	diameter of spherical particle (m)
D	spacing between parallel plates, and distance between centers of adjacent particles
f	number of particles present in the unit volume V_u
F_l	drag force on one particle (N)
g	gravitational acceleration ($m\,s^{-2}$)
$\bar{h}$	averaged heat transfer coefficient ($W\,m^{-2}\,K^{-1}$)
H	height (m)
k	fluid thermal conductivity ($W\,m^{-1}\,K^{-1}$)
k_m	porous medium thermal conductivity ($W\,m^{-1}\,K^{-1}$)
K	permeability (m^2)
L	length in the flow direction (m)
$\dot{m}$	mass flow rate ($kg\,s^{-1}$)
N	number of particles in volume AL
N_V	number of particles per unit volume (m^{-3})
q	heat transfer rate (W)
q_l	heat transfer rate from one particle (W)
q'''	heat transfer rate density ($W\,m^{-3}$)
Ra_p	porous medium Rayleigh number Eq. (41)
T_w	surface temperature (K)
T_0	initial fluid temperature (K)
u	volume averaged velocity ($m\,s^{-1}$)
u_p	free stream velocity ($m\,s^{-1}$)
U	mean fluid velocity in channel ($m\,s^{-1}$)
V	volume (m^3)
V_u	unit volume (m^3)
W	width (m)

Greek symbols

α	fluid thermal diffusivity ($m^2\,s^{-1}$)
α_m	porous medium thermal diffusivity ($m^2\,s^{-1}$)
β	coefficient of volumetric thermal expansion (K^{-1})
ΔP	pressure drop ($N\,m^{-2}$)
μ	viscosity ($kg\,s^{-1}\,m^{-1}$)
ν	kinematic viscosity ($m^2\,s^{-1}$)
ρ	density ($kg\,m^{-3}$)
ϕ	porosity

Subscripts

max	maximum
opt	optimum

Superscript

$(\tilde{})$	dimensionless variables, Eqs. (11) and (24)

where laminar fully developed flow is a routine design feature (e.g., [3–6]).

The best choice is in-between, $L \approx X_T$, because in this configuration all the fluid of the channel cross-section is active in a heat transfer sense. The fluid leaves the channel as soon as it completes its mission, i.e., as soon as the boundary layers have merged. In this configuration the channel volume is used to the maximum for the purpose of transferring heat between the stream and the walls. This principle has been used to optimize spacings in several channel configurations with natural and forced convection: volumes filled with a stack of continuous or staggered parallel plates, volumes filled with parallel cylinders in crossflow, and three-dimensional pin fin arrays with impinging flow [7–23]. These results have been summarized in [1,2,25,26].

The simplest example of geometric optimization for forced convection was the optimization of the spacing between parallel-plates channels that fill a larger volume [11]. With reference to the lower drawing of Fig. 1, when the pressure difference between the two ends of the channel is specified (ΔP), maximal heat transfer rate per unit volume is achieved when

$$\frac{D_{opt}}{L} \cong 2.73 Be_L^{-1/4} \tag{1}$$

where Be_L is the pressure difference number based on the flow length L, which Bhattacharjee and Grosshandler [27] and Petrescu [28] termed the Bejan number,

$$Be_L = \frac{\Delta P L^2}{\mu \alpha} \tag{2}$$

The corresponding maximal average heat transfer rate per unit of channel volume is

$$q'''_{max} \lesssim 0.62 \frac{k}{L^2}(T_w - T_0) Be_L^{1/2} \tag{3}$$

where $(T_w - T_0)$ is the temperature difference between the plate surfaces and the entering single-phase coolant.

Eqs. (1)–(3) result from the *intersection of asymptotes method*, in which q''' is estimated analytically in two extremes: (a) narrow spacings, in which the flow through the channel is in the Hagen–Poiseuille regime, and (b) wide spacings, where the channel is thicker than the boundary layers. The intersection of asymptotes (a) and (b) yields Eqs. (1) and (3). The inequality sign in Eq. (3)

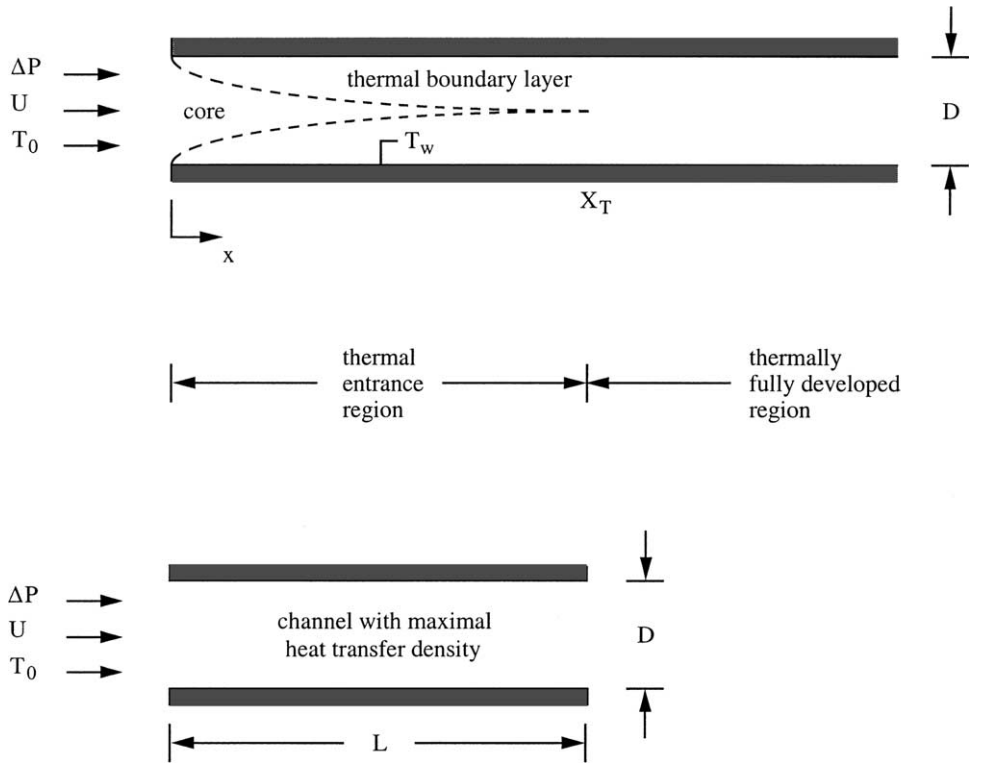

Fig. 1. Maximal heat transfer rate per unit volume is achieved when the channel length matches the thermal entrance length of the flow.

is a reminder that the intersection of (a) and (b) provides a $q'''_{\max}$ estimate that falls above the actual peak of the $q'''(D)$ curve. Numerical maximizations of q''' vs. D confirm the analytical form of Eq. (3), and show that the factor 0.62 should be replaced by 0.4 [11,29].

The intersection of asymptotes method and scale analysis were developed as problem solving methods for convection in 1984 [8]. Additional applications of the intersection of asymptotes method are presented in [1,2], and in the 1995 edition of [8]. The accuracy, generality and mathematical basis of the intersection of asymptotes method were discussed most recently by Lewins [30].

The new work reported in this paper is in response to the message furnished by Eq. (3). The volumetric density of heat transfer rate can be increased by decreasing L, because $q'''_{\max}$ is proportional to L^{-1}. Smaller and smaller dimensions are attractive. According to Eq. (1), however, D is proportion to $L^{1/2}$. This means that the aspect ratio D/L is proportional to $L^{-1/2}$, and the channel becomes less slender when the size L becomes smaller. In this limit of increasing D/L ratios, the boundary layer slenderness assumption on which asymptote (b) and Eqs. (1)–(3) are based breaks down.

The fundamental question then is this: What are the design rules for channels with maximal heat transfer density when dimensions are so small that Eqs. (1)–(3) do not apply? This question is important because the push for maximal heat transfer rate densities, which generated Eqs. (1)–(3), continues undiminished toward smaller dimensions.

2. Optimal geometry in the small-scales limit

Consider the limit of dimensions (L, D) so small that D/L is not much smaller than 1. Boundary layer theory does not hold. If the channels are sufficiently wide to be surrounded completely by cold fluid (T_0), then the heat transfer from each plate to the fluid is by quasi-radial conduction. This regime is shown in Fig. 2(b). In the other extreme, Fig. 2(a), where dimensions are again small, but, in addition, the channels that fill the fixed volume of the package (HL^2) are many, the flow through each channel is in the Hagen–Poiseuille regime. In regime (a) the mean velocity is

$$U = \frac{D^2}{12\mu}\frac{\Delta P}{L} \tag{4}$$

The total flow rate through the HL^2 volume is $\dot{m} = \rho HLU$. The total enthalpy increase experienced by the $\dot{m}$ stream is $q = \dot{m}c_P(T_w - T_0)$, because in this limit the spacing D is so tight, and the wall-fluid thermal contact

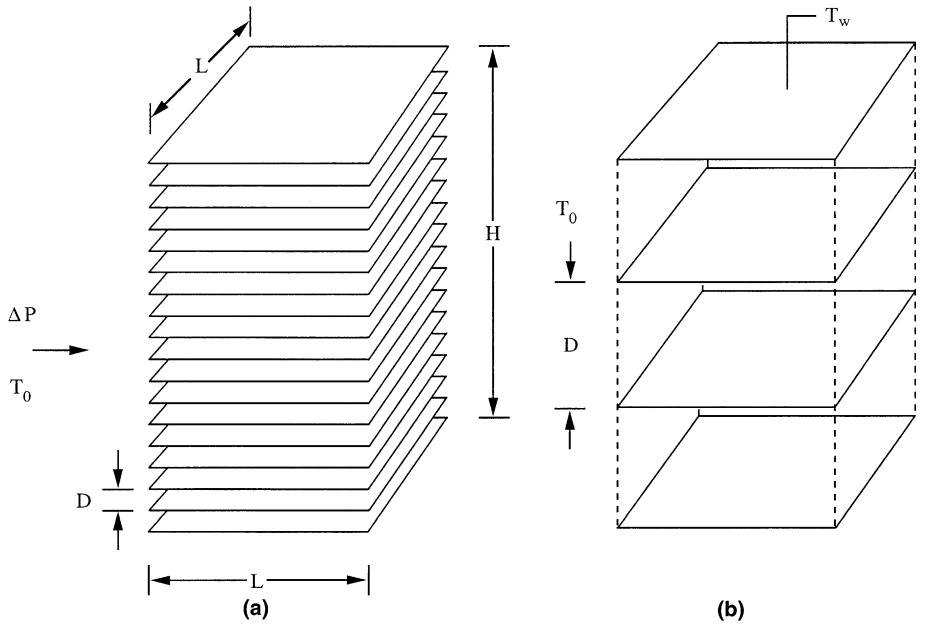

Fig. 2. Stack of parallel plates: (a) the small-D limit, and (b) the large-D limit.

so good, that the outlet temperature of the $\dot{m}$ stream is essentially equal to the plate temperature T_w. The volumetric heat transfer density is $q''' = q/(HL^2)$, or

$$q''' = \frac{D^2 \Delta P}{12 \nu L^2} c_p (T_w - T_0) \tag{5}$$

In the opposite extreme, Fig. 2(b), each plate is surrounded by T_0 fluid, because convection is negligible. In the limit of small linear dimensions, the rate of heat transfer from one plate to the fluid (q_1) is proportional to $Lk(T_w - T_0)$, where L is the linear dimension of the plate. We can use a more accurate q_1 estimate by noting that if q_1 emanates from a T_w disc of diameter d immersed in a medium at T_0, then q_1 is given by (cf. [31, p. 119])

$$q_1 = 4dk(T_w - T_0) \tag{6}$$

In the configuration of Fig. 2(b) the plate area is L^2 instead of $\pi d^2/4$, which means that in Eq. (5) we may replace d approximately with $(4/\pi)^{1/2} L$. Next, the total heat transfer rate emanating from the stack is $q = Nq_1$, where $N = H/D$ is the number of plates in the stack. Finally, the volumetric rate of heat transfer is $q''' = q/(HL^2)$, which becomes

$$q''' = \frac{8k(T_w - T_0)}{\pi^{1/2} DL} \tag{7}$$

In summary, asymptotes (5) and (7) show that q''' can be maximized with respect to D. Eq. (5) holds when D is small, and shows that q''' decreases as D decreases. Eq. (7) holds when D is large, and shows that q''' decreases as D increases. This asymptotic behavior guarantees that q''' reaches a maximum in the vicinity of the intersection of Eqs. (5) and (7). The optimal spacing and maximal heat transfer density are

$$\frac{D_{opt}}{L} \cong 3.78 Be_L^{-1/3} \tag{8}$$

$$q'''_{max} \lesssim 1.2 \frac{k}{L^2} (T_w - T_0) Be_L^{1/3} \tag{9}$$

Eq. (9) shows that q''' increases as $L^{-4/3}$ as L decreases. This increase is faster in comparison with the behavior of q''' at larger scales, Eq. (3), where q'''_{max} increases as L^{-1} as L decreases. This change in the behavior of q'''_{max} stresses not only the importance of seeking smaller dimensions, but also the importance of knowing the correct scaling laws when dimensions have become small enough.

The transition from the large-scales optimum to the small-scales optimum is obtained by intersecting Eqs. (1) and (8), or Eqs. (3) and (9). In either case, the transition is found to occur at

$$Be_L^{1/2} \approx 8 \tag{10}$$

where $Be_L^{1/2} \lesssim 8$ is the domain of validity of the small-scales solution, Eqs. (8) and (9). The number $Be_L^{1/2}$ represents a dimensionless flow length L when ΔP is specified. This observation recommends the use of the dimensionless variables

$$\begin{aligned} (\tilde{D}, \tilde{L}) &= (D, L) \left(\frac{\Delta P}{\mu \alpha} \right)^{1/2} \\ \tilde{q}''' &= \frac{q''' \mu \alpha}{\Delta P k (T_w - T_0)} \end{aligned} \tag{11}$$

where $\widetilde{L}$ is the same as $Be_L^{1/2}$. These dimensionless variables transform Eqs. (1) and (8) into

$$\widetilde{D}_{opt} \cong 2.73\widetilde{L}^{1/2} \tag{12}$$

$$\widetilde{D}_{opt} \cong 3.78\widetilde{L}^{1/3} \tag{13}$$

and Eqs. (3) and (9) into

$$\tilde{q}'''_{max} \lesssim 0.62\widetilde{L}^{-1} \tag{14}$$

$$\tilde{q}'''_{max} \lesssim 1.2\widetilde{L}^{-4/3} \tag{15}$$

These two sets of asymptotes are displayed in Fig. 3. The heat transfer density increases in accelerated fashion as the length scale $\widetilde{L}$ decreases. In the same direction, the decrease of $\widetilde{D}_{opt}$ slows down. The transition from large scales to small scales occurs in the vicinity of $\widetilde{L} \approx 8$, where the channel slenderness ratio is $\widetilde{D}_{opt}/\widetilde{L} \sim 1$, in accordance with the threshold below which the boundary layers in the entrance region (Fig. 1) breaks down.

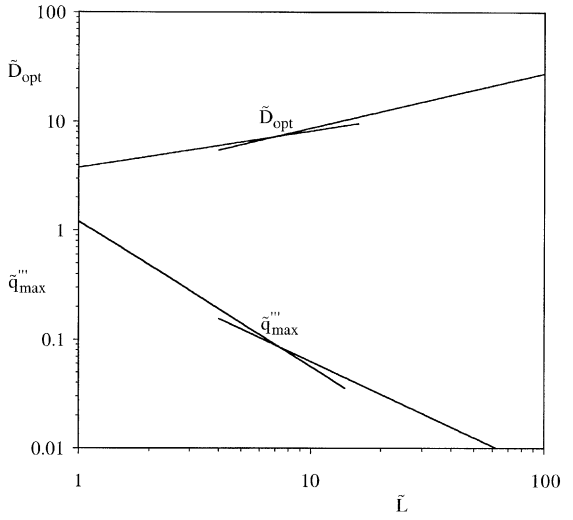

Fig. 3. The effect of the decreasing length scale ($\widetilde{L}$) on the optimal spacing and maximal heat transfer rate density.

3. Packed spheres

Optimal spacings represent optimal packing. In the case of Fig. 2, the volume H^2L is packed optimally with parallel plates when the spacing is selected in accordance with Eqs. (1) and (8). The optimization of packing is pursued in another generic configuration in Fig. 4. The volume $V = AL$ contains a number (N) of heat-generating spheres of diameter d and temperature T_w. The coolant that bathes this volume has the inlet temperature T_0. The flow is driven by the pressure gradient $\Delta P/L$. The objective is to maximize the heat transfer rate density (q''') when T_w, T_0 and other flow parameters are fixed. The key variable is the spacing between spheres, which is related to varying N, or the porosity of the system,

$$\phi = 1 - \frac{\pi N d^3}{6V} \tag{16}$$

The intersection of asymptotes method consists of determining q''' in two extremes, tight spaces (Fig. 4a) and large spaces (Fig. 4b), and intersecting the two asymptotes. When spaces are tight, and if the flow is slow enough for the Darcy model to be valid, the volume averaged fluid velocity in the L direction is

$$u = \frac{K}{\mu}\frac{\Delta P}{L} \tag{17}$$

where K is the permeability of the porous medium that resides inside V. In the same slow-flow limit, the outlet temperature of the fluid is essentially equal to the temperature of the solid particles, T_w. The total heat transfer rate from solid to fluid is $q = \rho u A c_p (T_w - T_0)$. The corresponding heat transfer density is $q''' = q/V$, which after using Eq. (17) becomes

$$q''' = \frac{\rho c_p K \Delta P}{\mu L^2}(T_w - T_0) \tag{18}$$

When the spheres are far apart, and if the flow is so slow that convection is negligible relative to conduction in the spaces between spheres, then an adequate heat transfer estimate can be made based on the assumption

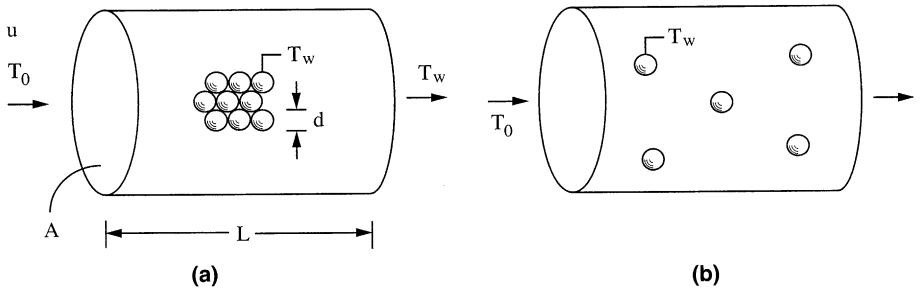

Fig. 4. Spheres packed in a fixed space: (a) small spacings, and (b) large spacings.

of pure conduction. The steady-state heat transfer rate from one sphere is (e.g., [31])

$$q_1 = 2\pi kd(T_w - T_0) \tag{19}$$

The total heat transfer rate ($q = Nq_1$) leads to the heat transfer density $q''' = q/V$, which in view of Eq. (16) is

$$q''' = \frac{12}{d^2}(1-\phi)k(T_w - T_0) \tag{20}$$

To summarize, Eq. (20) shows that when spacings are large the heat transfer density decreases as the spacings (or ϕ) increase. In the other extreme, Eq. (18) shows that when spaces are tight and continue to decrease, q''' decreases because the permeability decreases. The mid-range where q''' reaches its maximum is identified by intersecting Eqs. (18) and (20),

$$\frac{K_{opt}\Delta P}{\alpha\mu L^2} = \frac{12}{d^2}(1-\phi_{opt}) \tag{21}$$

The optimal packing is characterized by the permeability K_{opt} and porosity ϕ_{opt}. Assuming that porosities are not almost equal to 1, parameters K and ϕ are related in accordance with the Carman–Kozeny theory [32],

$$K = \frac{d^2\phi^3}{180(1-\phi)^2} \tag{22}$$

in which 180 is an empirical constant. Then, Eq. (21) pinpoints the optimal porosity of the system,

$$\left(\frac{1}{\phi_{opt}} - 1\right)\frac{\tilde{L}^{2/3}}{\tilde{d}^{4/3}} = 0.0774 \tag{23}$$

where, in accordance with the nondimensionalization method chosen in Eq. (11),

$$(\tilde{d}, \tilde{L}) = (d, L)\left(\frac{\Delta P}{\mu\alpha}\right)^{1/2} \tag{24}$$

The optimal porosity ϕ_{opt} is a function of $\tilde{d}^2/\tilde{L}$. This curve is labeled "Eq. (22)" in Fig. 5 because it is based on the Carman–Kozeny correlation (22).

The optimal spacing between particles can be calculated after making an assumption regarding the geometric arrangement. If the spheres are placed in a cubic arrangement with the distance D between centers, then the porosity is

$$\phi = 1 - \frac{\pi}{6}\left(\frac{d}{D}\right)^3 \tag{25}$$

By eliminating ϕ between Eqs. (23) and (25), we find the optimal relative spacing D/d, as a function of the group $\tilde{d}^2/\tilde{L}$. This function is labeled "Eq. (22)" in Fig. 6. The spacing increases as $\tilde{d}^2/\tilde{L}$ decreases, i.e., in the same direction as $\phi_{opt} \to 1$. The smallest porosity occurs when the particles touch, namely, $\phi = 0.4764$ when $D/d = 1$.

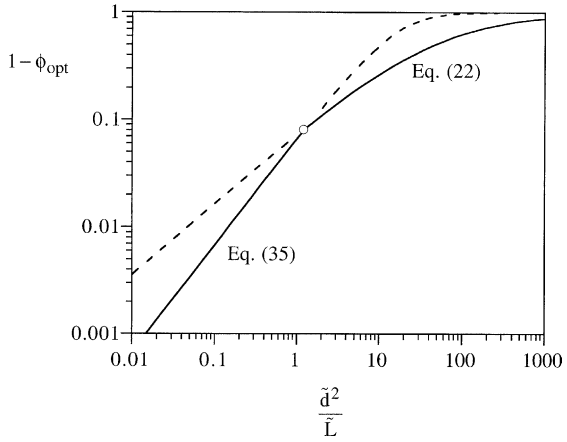

Fig. 5. The optimized porosity of the volume packed with spheres and maximal heat transfer rate density.

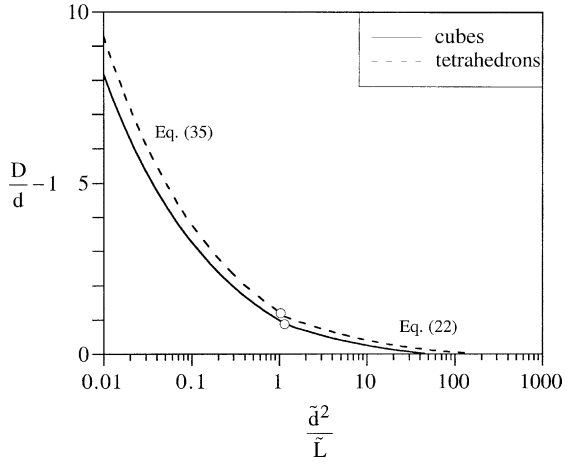

Fig. 6. The optimized distance between particle centers.

If the spherical particles are arranged more tightly so that their centers are the corners of tetrahedrons, then the porosity of the medium is

$$\phi = 1 - \frac{\pi}{2^{1/2}3}\left(\frac{d}{D}\right)^3 \tag{26}$$

Eqs. (23) and (26) yield the relative size of the side of the tetrahedron. This result is shown with dashed line in Fig. 6. When the spheres touch the porosity is 0.26. The effect of the geometric arrangement in the packing is small; spacings are larger when the particle centers form tetrahedrons.

The maximal heat transfer rate density that corresponds to the design optimized above is

$$\tilde{q}'''_{max} \lesssim \frac{12}{\tilde{d}^2}(1-\phi_{opt}) \tag{27}$$

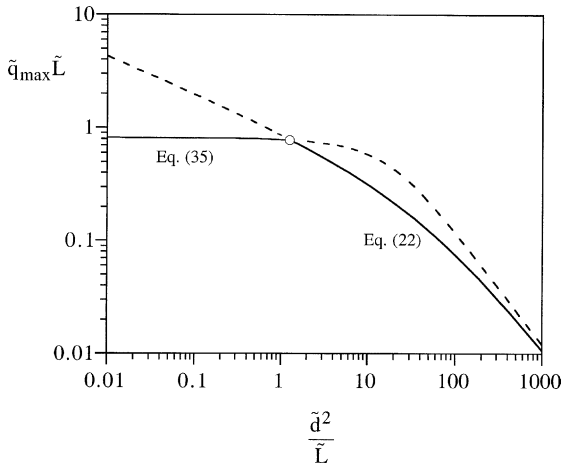

Fig. 7. Upper bounds for the maximal heat transfer rate density in a volume packed uniformly with spherical particles.

Note again that the inequality sign is due to the intersection of asymptotes method. The right-hand side of Eq. (27) is the correct order of magnitude of $\tilde{q}'''_{\max}$, which shows the strong effect that the particle size has on the heat transfer density. The heat transfer rate density increases substantially as the smallest dimension of the configuration ($\tilde{d}$) becomes smaller. The optimal porosity increases in the same direction. Eqs. (27) and (23) can be combined to eliminate ϕ_{opt}, and to reveal $\tilde{q}'''_{\max}$ as a function of the internal and external dimensions $(\tilde{d}, \widetilde{L})$. See the curve labeled "Eq. (22)" in Fig. 7: the heat transfer rate density increases as $\widetilde{L}$ decreases.

4. Sparsely distributed particles

In summary, a structure with smaller d and larger ϕ values is better. This points in the direction of sparsely distributed particles $\phi \to 1$, where the preceding results [Eqs. (23)–(27)] are, at best, valid only approximately because they are based on the Carman–Kozeny correlation (22). We analyze this limit in order to shed light on the optimization of man-made porous structures, for which, in many cases, $\phi \to 1$. In the present analysis, the sparse distribution of spherical particles plays the role of simple model, i.e., a facsimile with a very small number of dimensions, which accounts qualitatively for multi-dimensional man-made porous structures.

The dimensions are the same as in the preceding section: d, D and L. The difference is that in the $\phi \to 1$ limit we may regard the flow around each particle as independent of the flow around neighboring particles. Furthermore, we assume that the particle size is so small that the Reynolds number $u_p d/\nu$ is smaller than 1, and, the sphere drag coefficient is given by Stokes flow solution

$$C_D = \frac{24}{u_p d/\nu} \tag{28}$$

Here u_p is the free stream velocity in the fluid space,

$$u_p = \frac{u}{\phi} \tag{29}$$

and u is the volume averaged velocity used in Eq. (17). The drag experienced by one particle is

$$F_1 = \frac{24}{u_p d/\nu}\frac{1}{2}\rho u_p^2 \frac{\pi}{4} d^2 \tag{30}$$

The longitudinal force balance on the volume AL shown in Fig. 4 requires

$$N_V A L F_1 = A \Delta P \tag{31}$$

where N_V is the number of particles present per unit volume. By combining Eq. (31) with Eqs. (28)–(30) we obtain an expression for $\Delta P/L$, which can be compared with the Darcy law (17). From this comparison results the permeability formula

$$K = \frac{\phi}{3\pi d N_V} \tag{32}$$

The number N_V depends on the geometric arrangement. For example, in the cubic arrangement $N_V = 1/V_u$, where $V_u (= D^3)$ is the unit volume represented by one cube of side D. In the case of a tetrahedron of unit volume V_u, the corresponding number is $N_V = (1/6)/V_u$. To keep the analysis general, we write that

$$N_V = \frac{f}{V_u} \tag{33}$$

where f is the fraction of one particle that belongs to one unit volume V_u (namely, $f = 1$ for cube, and $f = 1/6$ for tetrahedron). The porosity can also be expressed in terms of N_V,

$$\phi = \frac{V_u - f\frac{\pi}{6}d^3}{V_u} = 1 - N_V \frac{\pi}{6} d^3 \tag{34}$$

such that Eqs. (32) and (34) yield

$$K = \frac{d^2}{18}\frac{\phi}{1-\phi} \tag{35}$$

This is the theoretical permeability for any arrangement of spheres when $\phi \lesssim 1$ and $u_p d/\nu < 1$. It replaces Eq. (22) in the analysis shown in the preceding section, and the new results are presented as curves "Eq. (35)" in Figs. 5–7. Qualitatively, the trends are the same. For example, in place of Eq. (23), the optimal porosity is given by

$$\frac{1-\phi_{\text{opt}}}{\phi_{\text{opt}}^{1/2}} = (216)^{-1/2}\frac{\tilde{d}^2}{\widetilde{L}} \tag{36}$$

This curve has been added to Fig. 5. We see again that the optimal porosity increases as the particle size decreases. The corresponding spacing between particle centers is shown in Fig. 6.

Eq. (27) holds unchanged in the $\phi \to 1$ limit. By combining it with Eq. (36), and making the approximation $\phi_{\text{opt}}^{1/2} \approx 1$, we reach the important conclusion that in the $\phi \to 1$ limit the maximal heat transfer density becomes independent of particle size,

$$\tilde{q}'''_{\max} \lesssim \frac{(2/3)^{1/2}}{\widetilde{L}} \tag{37}$$

This formula is plotted as "Eq. (35)" in Fig. 7. The $\widetilde{L}$ dependence exhibited by $\tilde{q}'''_{\max}$ is qualitatively the same as in Eq. (15), i.e., the same as when the volume is packed with heat transfer distributed on parallel plates.

5. Optimal spacings for channels filled with a porous structure

The optimization of spacings in the limit of decreasing length scales leads to flow structures that look more and more like porous structures with 'designed' pores. The development of such structures defines a field that may be regarded as *designed porous media* [2]. In this section we cover another fundamental configuration of designed porous media, namely, the optimization of spacings between plates that sandwich a porous medium. For example, the channels may be occupied by a metallic foam (e.g., [33,34]) such that the saturated porous medium has a thermal conductivity (k_{m}) and a thermal diffusivity (α_{m}) that are much higher than their pure fluid properties (k, α), which were used in Sections 2–4. We consider both natural convection and forced convection with Boussinesq incompressible fluid, and assume that the structures are fine and thick enough that Darcy flow prevails in all cases.

The natural convection configuration is shown in Fig. 8, which is the same as Fig. 2a with the plates oriented vertically. This time each D-thin space is filled with the assumed fluid saturated porous structure. The width in the direction perpendicular to Fig. 8 is W. The effective pressure difference that drives the flow is due to buoyancy,

$$\Delta P = \rho H g \beta (T_{\text{w}} - T_0) \tag{38}$$

This ΔP estimate is valid in the limit where the spacing D is sufficiently small that the temperature in the channel porous medium is essentially the same as the plate temperature T_{w}. In this limit, the heat current extracted by the flow from the $H \times L$ volume is $q = \dot{m} c_{\text{p}} (T_{\text{w}} - T_0)$, with $\dot{m} = \rho ULW$ and, according to Darcy's law,

$$U = K \Delta P / (\mu H) \tag{39}$$

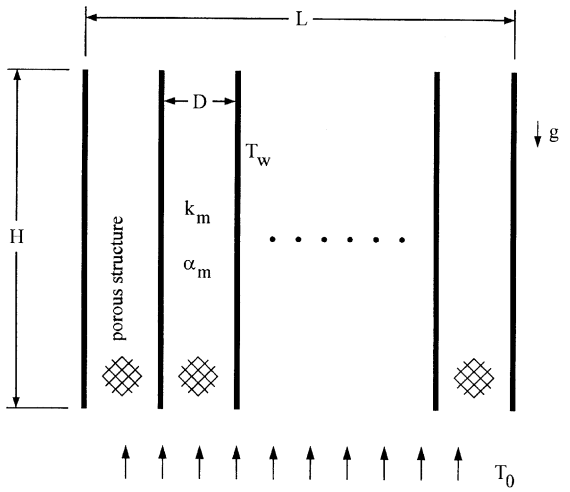

Fig. 8. Volume filled with vertical heat-generating plates separated by a fluid saturated porous medium.

where K is the permeability of the structure. In conclusion, the total heat transfer rate in the small-D limit is independent of the spacing D

$$q = \rho c_{\text{p}} (T_{\text{w}} - T_0) LW (K \Delta P) / (\mu H) \tag{40}$$

In the opposite limit, D is large enough so that the natural convection boundary layers that line the H-tall plates are distinct. The heat transfer rate from one boundary layer is $\bar{h} HW (T_{\text{w}} - T_0)$, where the classical result (e.g., [26,31]) for the average heat transfer coefficient is $\bar{h} H / k_{\text{m}} = 0.888 Ra_{\text{p}}^{1/2}$, and Ra_{p} is the Rayleigh number for Darcy flow,

$$Ra_{\text{p}} = Kg\beta H (T_{\text{w}} - T_0) / (\alpha_{\text{m}} \nu) \tag{41}$$

The number of boundary layers in the $H \times L$ volume is $2L/D$. In conclusion, the total heat transfer rate decreases as D increases (see Fig. 9)

$$q = 1.78 (L/D) W k_{\text{m}} (T_{\text{w}} - T_0) Ra_{\text{p}}^{1/2} \tag{42}$$

The effect of the spacing (Fig. 9) requires discussion. For maximal thermal conductance $q/(T_{\text{w}} - T_0)$, the spacing D must be smaller than the estimate obtained by intersecting asymptotes (40) and (42):

$$D_{\text{opt}} / H \lesssim 1.78 Ra_{\text{p}}^{-1/2} \tag{43}$$

The simplest design that has the highest possible conductance is the design with the fewest plates, i.e., the largest D_{opt}, hence $D_{\text{opt}} / H \cong 1.78 Ra_{\text{p}}^{-1/2}$ for the recommended design. Contrary to Fig. 9, however, q does not remain constant as D decreases indefinitely. There must exist a small enough D below which the passages are so tight (tighter than the pores) that the flow stops. An estimate for how large D should be so that Eq. (43) is valid is obtained by requiring that the D_{opt} value for

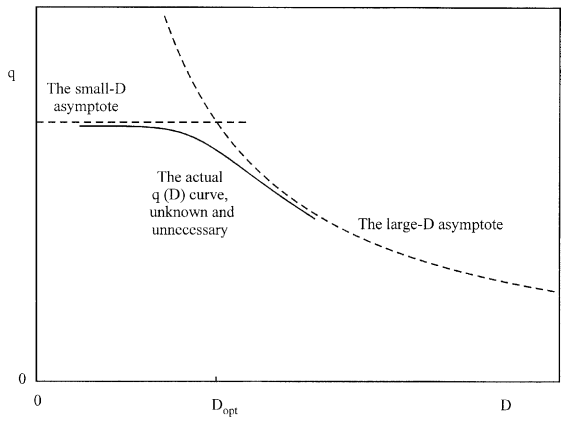

Fig. 9. The effect of the channel spacing on the global thermal conductance when the channels are filled with a fluid-saturated porous structure.

natural convection when the channels are filled only with fluid [8,26],

$$D_{opt}/H \cong 2.3[g\beta H^3(T_w - T_0)/(\alpha\nu)]^{-1/4} \tag{44}$$

must be smaller than the D_{opt} value of Eq. (43). We find that this is true when

$$\frac{H^2}{K}\frac{\alpha_m}{\alpha} > Ra_p \tag{45}$$

in which, normally, $\alpha_m/\alpha \gg 1$ and $H^2/K \gg 1$.

The forced convection configuration can be optimized similarly. The flow is driven by the imposed ΔP through parallel-plates channels of length L and width W. The thermal conductance in the small-D limit is the same as in Eq. (40). In the large-D limit there are $2H/D$ distinct boundary layers, and the heat transfer rate across one boundary layer is $\bar{h}LW(T_w - T_0)$. The L-averaged heat transfer coefficient is [26]: $\bar{h}L/k_m = 1.128(UL/\alpha_m)^{1/2}$. Putting these formulas together, we find that in the large-D limit the global thermal conductance is

$$q = 2.26(H/D)Wk_m(T_w - T_0)(UL/\alpha_m)^{1/2} \tag{46}$$

The forced-convection asymptotes (10) and (46) have the same behavior as in Fig. 9. The highest conductance occurs to the left of the intersection of the two asymptotes, when

$$D_{opt}/L \lesssim 2.26Be_p^{-1/2} \tag{47}$$

and where Be_p is the Bejan number for the porous medium,

$$Be_p = (\Delta PK)/(\mu\alpha_m) \tag{48}$$

This forced-convection optimization is valid when the D_{opt} estimate for the channel with pure fluid [Eq. (1)] is smaller than the D_{opt} value provided by Eq. (47), i.e., when

$$\frac{L^2}{K}\frac{\alpha_m}{\alpha} > Be_p \tag{49}$$

In summary, Eqs. (43) and (47) provide estimates for the optimal spacings when the channels between heat-generating plates are filled with a fluid-saturated porous structure. The relevant dimensionless groups are Ra_p, Be_p, K/H^2, K/L^2 and α_m/α. The symmetry between Eqs. (43) and (47), and between Eqs. (45) and (49), reinforces Petrescu's [28] argument that the role of the Bejan number in forced convection is analogous to that of the Rayleigh number in natural convection.

6. Conclusions

This paper addressed the fundamental question of how to maximize the density of heat transfer rate in a finite-size volume. The new aspect of this work is the limit of decreasing length scales. In this limit boundary layers disappear, and existing solutions [7–26] for the maximization of heat transfer rate density are not valid. The maximization of heat transfer rate density in the limit of decreasing scales is key to the continued miniaturization of heat transfer devices.

This work revealed several important and fundamental results. First, it showed that it is possible to optimize the internal spacings of volumes with forced convection when boundary layers disappear. This was demonstrated for two configurations, a volume filled with parallel plates, and a volume packed with spheres of one size. Furthermore, volumes packed with spheres were optimized here for the first time, because unlike the parallel-plates and other configurations [7–26], they had not been optimized at large scales where boundary layers are present.

Each configuration is characterized by three length scales: (i) the external dimension of the volume, which is measured in the flow direction (L), (ii) the thickness of the solid elements (plate thickness, sphere diameter), and (iii) the internal dimension represented by the size of the channel through which the fluid flows (the spacing D, or the porosity of the assembly). Dimension (iii) was optimized for maximal heat transfer rate density, while dimensions (i) and (ii) were specified. The optimized configuration showed how the internal flow spaces change as the dimensions (i) and (ii) continue to decrease. The overall performance increases as dimensions become smaller.

In the case of volumes filled with parallel-plates channels, the small-scales solution becomes valid when the external dimension $\tilde{L}$ becomes smaller than 8. In the small-scales limit, the heat transfer rate density increases as $\tilde{L}^{-4/3}$, which is a faster increase than at larger scales

where boundary layers are present. In the small-scales limit the optimal spacing D is larger than the plate length L, and the ratio D/L increases as $\tilde{L}^{-2/3}$.

Volumes filled with solid spheres are porous media the porosities of which can be optimized. We showed this by using two models for the permeability of the medium, the Carman–Kozeny correlation, Eq. (22), and the theoretical limit of Stokes flow around isolated spheres, Eq. (35). By assuming certain arrangements for the centers of the spheres (e.g., cube, tetrahedron), the optimal porosity is translated into an optimal spacing between spheres. The optimal porosity approaches 1 as the group $\tilde{d}^2/\tilde{L}$ decreases. In the same limit, the maximal heat transfer rate density varies as $\tilde{L}^{-1}$, and is independent of the sphere size.

Section 5 reported the development of optimal spacings for channels filled with a fluid-saturated porous structure. The results are the most fundamental, and are based on a simple model and a simple analysis: Darcy flow, and the intersection of asymptotes method. The same idea of geometry optimization deserves to be pursued in future studies, based on more refined models and more accurate methods of flow simulation.

In particular, the analytical approach illustrated in this paper can be refined by basing the porous medium model on the new work that has been emerging on channels filled with coarse metallic porous structures, e.g. [33,34]. For example, the present models did not include features that account for the connectivity of the solid parts and conduction along the solid. This was done for two reasons, simplicity and design.

Simplicity was chosen because it is the most effective way of explaining new ideas. It is true that the same ideas can be explored in more specific cases and regimes of operation, where additional modeling features may have to be taken into account. The contribution of simplicity is this: the opportunities to optimize morphing flow architectures (constructal design) become clear even in the nakedly simple models that one finds in the introductory textbooks. It is in this way that the constructal principle of flow architecture becomes textbook material.

Design is the main feature of the structures analyzed in this paper. These structures begin to look like "designed porous media" [2] only in the limit of decreasing dimensions, when the macroscopic (human) scale of the device remains fixed. Such structures should not be confused with naturally occurring porous media, in which the solid connectivity question may be raised even earlier. The designer is entitled to contemplate the maximization of heat transfer packing while looking at drawings such as Figs. 1, 2 and 4, where the solid parts are not connected. The manufacturing of the optimized structure is a subsequent step, which, if it shows the need for extensive solid–solid connections, may recommend a subsequent look at the constructal design of structure. But even without such a recommendation, to include additional modeling features is a very good idea for a future fundamental study on the path opened by this paper.

In summary, we traced in very simple terms the route to the highest density of heat transfer rate when dimensions continue to decrease. The route consists of optimizing the internal geometry of the device. The method is a continuation of what has been used at larger scales, where boundary layers are present and optimized channels are slender [1,2]. The method applies at small scales, as long as the continuum model holds. But even before the continuum description breaks down, surface effects such as electrokinetics in liquid flow [35] will have to be taken into account.

Acknowledgements

This work was supported by a grant from the National Science Foundation. The author acknowledges with gratitude the comments and support received on this paper from Prof. S. Lorente, Prof. A.F. Miguel, Prof. A.H. Reis, Prof. I. Dincer, Prof. L.A.O. Rocha, Prof. J.C. Ordonez and Mr. A.K. da Silva.

References

[1] A. Bejan, Shape and Structure, from Engineering to Nature, Cambridge University Press, Cambridge, UK, 2000.
[2] A. Bejan, I. Dincer, S. Lorente, A.F. Miguel, A.H. Reis, Porous and Complex Flow Structures in Modern Technologies, Springer, New York, 2004.
[3] R.W. Knight, J.S. Goodling, D.J. Hall, Optimal thermal design of forced convection heat sinks–analytical, J. Electron. Packag. 113 (1991) 313–321.
[4] A. Bar-Cohen, A.D. Kraus, Advances in Thermal Modeling of Electronic Components and Systems, vol. 2, ASME Press, New York, 1990.
[5] A.B. Duncan, G.P. Peterson, Review of microscale heat transfer, Appl. Mech. Rev. 47 (1994) 397–428.
[6] P. Gao, S. Le Person, M. Favre-Marinet, Scale effects on hydrodynamics and heat transfer in two-dimensional mini and microchannels, Int. J. Therm. Sci. 41 (2002) 1017–1027.
[7] A. Bar-Cohen, W.M. Rohsenow, Thermally optimum spacing of vertical natural convection cooled, parallel plates, J. Heat Transfer 106 (1984) 116–123.
[8] A. Bejan, Convection Heat Transfer, Wiley, New York, 1984, problem 11, p. 157; Solutions Manual, pp. 93–95.
[9] W. Nakayama, H. Matsushima, P. Goel, Forced convective heat transfer from arrays of finned packages, in: W. Aung (Ed.), Cooling Technology for Electronic Equipment, Hemisphere, New York, 1988, pp. 195–210.
[10] N.K. Anand, S.H. Kim, L.S. Fletcher, The effect of plate spacing on free convection between heated parallel plates, J. Heat Transfer 114 (1992) 515–518.

[11] A. Bejan, E. Sciubba, The optimal spacing of parallel plates cooled by forced convection, Int. J. Heat Mass Transfer 35 (1992) 3259–3264.
[12] H. Matsushima, T. Yanagida, Y. Kondo, Algorithm for predicting the thermal resistance of finned LSI packages mounted on a circuit board, Heat Transfer Jpn. Res. 21 (5) (1992) 504–517.
[13] A. Bejan, Al.M. Morega, The optimal spacing of a stack of plates cooled by turbulent forced convection, Int. J. Heat Mass Transfer 37 (1994) 1045–1048.
[14] W. Nakayama, Information processing and heat transfer engineering: some generic views on future research needs, in: S. Kakac, Y. Yüncü, K. Hijikata (Eds.), Cooling of Electronic Systems, Kluwer Academic Publishers, Dordrecht, The Netherlands, 1994, pp. 911–943.
[15] A. Bejan, A.J. Fowler, G. Stanescu, The optimal spacing between horizontal cylinders in a fixed volume cooled by natural convection, Int. J. Heat Mass Transfer 38 (1995) 2047–2055.
[16] A. Campo, G. Li, Optimum separation of asymmetrically heated sub-channels forming a bundle: influence of simultaneous flow and temperature, Heat Mass Transfer 32 (1996) 127–132.
[17] G. Stanescu, A.J. Fowler, A. Bejan, The optimal spacing of cylinders in free-stream cross-flow forced convection, Int. J. Heat Mass Transfer 39 (1996) 311–317.
[18] G. Ledezma, A.M. Morega, A. Bejan, Optimal spacings between pin fins with impinging flow, J. Heat Transfer 118 (1996) 570–577.
[19] B. Morrone, A. Campo, O. Manca, Optimum plate separation in vertical parallel-plate channels for natural convective flows: incorporation of large spaces at the channel extremes, Int. J. Heat Mass Transfer 40 (1997) 993–1000.
[20] G.A. Ledezma, A. Bejan, Optimal geometric arrangement of staggered vertical plates in natural convection, J. Heat Transfer 119 (1997) 700–708.
[21] A.J. Fowler, G.A. Ledezma, A. Bejan, Optimal geometric arrangement of staggered plates in forced convection, Int. J. Heat Mass Transfer 40 (1997) 1795–1805.
[22] M. Landon, A. Campo, Optimal shape for laminar natural convective cavities containing air and heated from the side, Int. Comm. Heat Mass Transfer 26 (1999) 389–398.
[23] A. Campo, Bounds for the optimal conditions of forced convective flows inside multiple channels whose plates are heated by a uniform flux, Int. Comm. Heat Mass Transfer 26 (1999) 105–114.
[24] R.S. Matos, J.V.C. Vargas, T.A. Laursen, F.E.M. Saboya, Optimization study and heat transfer comparison of staggered circular and elliptic tubes in forced convection, Int. J. Heat Mass Transfer 44 (2001) 3953–3961.
[25] S.J. Kim, S.W. Lee (Eds.), Air Cooling Technology for Electronic Equipment, CRC Press, Boca Raton, FL, 1995.
[26] A. Bejan, Convection Heat Transfer, Wiley, New York, 1995, pp. 132–136.
[27] S. Bhattacharjee, W.L. Grosshandler, The formation of a wall jet near a high temperature wall under microgravity environment, ASME HTD 96 (1988) 711–716.
[28] S. Petrescu, Comments on the optimal spacing of parallel plates cooled by forced convection, Int. J. Heat Mass Transfer 37 (1994) 1283.
[29] S. Mereu, E. Sciubba, A. Bejan, The optimal cooling of a stack of heat generating boards with fixed pressure drop, flow rate and pumping power, Int. J. Heat Mass Transfer 36 (1993) 3677–3686.
[30] J. Lewins, Bejan's Constructal theory of equal potential distribution, Int. J. Heat Mass Transfer 46 (2003) 1541–1543.
[31] A. Bejan, Heat Transfer, Wiley, New York, 1993, pp. 331–332.
[32] D.A. Nield, A. Bejan, Convection in Porous Media, second ed., Springer, New York, 1999.
[33] K. Boomsma, D. Poulikakos, The effects of compression and pore size variations on the liquid flow characteristics in metal foams, J. Fluids Eng. 124 (2002) 263–272.
[34] K. Boomsma, D. Poulikakos, On the effective thermal conductivity of a three dimensionally structured fluid-saturated metal foam, Int. J. Heat Mass Transfer 44 (2001) 827–836.
[35] J.H. Masliyah, Electrokinetic Transport Phenomena, AOSTRA Technical Publication Series no. 12, Alberta, Canada, 1994.